Vol. 4, No. 5 May 2014 ISSN 2225-7217
ARPN Journal of Science and Technology

http://www.ejournalofscience.org

Structural Control of Benchmark Buildings Equipped with Variable Stiffness Devices and Viscous Fluid Dampers

[1] Angeli Doliente Cabaltica, [2] Pham Nhan Hoa, [3] Chu Quoc Thang
[1,2,3] Department of Civil Engineering, International University - Vietnam National University - HCM
Quarter 6, Linh Trung Ward, Thu Duc District, Ho Chi Minh City, Viet Nam

[1] pnhoa@hcmiu.edu.vn, [2] angeli.dc@hcmiu.edu.vn, [3] cqthang@hcmiu.edu.vn

ABSTRACT

This paper presents benchmark structural controlled buildings for seismically excited nonlinear buildings. These buildings focus on three typical steel structures, 3-, 9- and 20-story buildings designed for the SAC project for Los Angeles, California. The goal of this study is to assess the efficiency of a model building configured with a semi-active controlled stiffness devices (S-CSD) and enhanced by passive viscous fluid dampers (P-VFD). Evaluation criteria, control constraints, and algorithms of variable stiffness devices (including Riccati Optimal Active Control Algorithm - ROAC, Pole Placement Algorithm, Instantaneous Control with Displacement and Velocity Feedback - ICDVF, and Instantaneous Optimal Active Closed-Loop Control Algorithm - IOAC) are presented in this paper for design problems. Control strategies in order to reduce the seismic response of the buildings may be either passive, semi-active, or a combination thereof (hybrid). The problems presented in this paper and the paper's problems fit into the category of hybrid control. A simulation program has been built up (with the help of MATLAB) and made available to facilitate comparison of the efficiency and merits of the various control strategies. The structural control theory is applied to the benchmark problems to illustrate some of the design challenges in numerical samples.

Keywords: *Benchmark problems, Structural Control, Semi-active control, Hybrid control, Dynamics of Structures*

1. INTRODUCTION

Energy dissipation devices in general have been widely applied to protect construction structures from seismic excitation. The background of the state-of-the-art on supplemental systems for seismic protection can be found in references by Soong and Spencer [2]. This solution has been proven to be much more economical than traditional methods which increases the column sections of a system. Dampers are installed in a structural system to resist its lateral motion without involving major building modification. In particular, passive viscous fluid dampers (P-VFDs) are one of the devices used popularly. When a structure is subjected to moderate seismic events, the passive linear viscous fluid dampers may be expected to gain desired responses. In addition, a structure with passive dampers is more reliable than another structure with semi-active dampers since it does not rely on electricity for power supply. However, if a structural system undergoes an intense seismic motion, the forces in the P-VFDs may be higher in order to achieve an acceptable performance. This may exceed capacity of the device, hence P-VFDs are suitable for buildings located on moderate seismic regions and having a less number of storeys [1].

Semi-active dampers attached to buildings correspond to tall buildings or systems enduring strong earthquake ground motion. The semi-active systems obviously require sensors for displacement and velocity or velocity and acceleration detection, control laws for controller, and standby energy in case of losing power for the systems during earthquake motion. The desired responses of retrofitting structures depend on capacity dampers or the highest force of dissipation dampers as well as active control algorithms for semi-active devices. Some research studies on semi-active control dampers include variable friction dampers found by Lyan-Ywan Lu [7], variable viscous fluid dampers described by Robert J. Mcnamara and Douglas P. Taylor [3], and controlled stiffness devices for controlling structures, considered as semi-active systems developed by Y. Ribakov [4]. Nevertheless, the force capacity of practical control stiffness dampers [4] is too small to control high-rise buildings.

A structure retrofitted with both passive viscous fluid dampers and semi-active controlled stiffness devices can be efficient to a longer earthquake motion range. As a matter of fact, a signal – one of dynamic responses of the structural building – for the working of semi-active dampers is set in systems in advance. P-VFDs are used to dissipate input energy within their capacity. When vital forces for a structure to resist output energy exceed maximum forces of P-VFD, semi-active controlled stiffness devices are activated.

In this article, the dynamic response of benchmark buildings equipped with pure P-VFDs, pure S-CSDs, or combination of P-VFDs and S-CSDs subjected to ground acceleration is investigated. The objectives of the study are (1) to develop a model and procedure to evaluate the dynamic structural performances corresponding to various benchmark problems, (2) to find optimum active algorithms for S-CSDs, and (3) to compare response reduction between various strategies.

2. BUILDINGS WITH PASSIVE VISCOUS FLUID DAMPERS AND SEMI-ACTIVE CONTROLLED STIFFNESS DEVICES

2.1 Equation of Motion for the Multi-Story Shear Frame

Consider a frame modeled as shear-frame structure subjected to an externally applied lateral forces $P_i(t)$ and earthquake excitations $w(t)$ equipped with r dampers P-VFDs and r dampers S-CSDs with bay width L, height H_i, elastic modulus E, and moment of inertia about the axis of bending I_b and I_c for the beams and columns, respectively (Fig 1). A_i is the brace cross section; m_i, c_i, and k_i are the mass, the viscous damping coefficient, and the lateral stiffness of the i^{th} floor (i=1, 2, …, n) respectively; $x_i(t)$ are the lateral displacement of structure and n is the number of story. If the beams are rigid [i.e., EI_b=0], the lateral stiffness of a column with ends is $12(EI_c)/H^3$. Thus, the stiffness of columns at the i^{th} floor is [6]:

$$k_i = \sum_{\text{columns}} \frac{12EI_c}{H^3} \qquad (1)$$

Through Newton's second law of motion, the differential equations governing the displacement $x_i(t)$ of such a structure system under earthquake excitation for each mass (Fig 2) are:

$$\begin{cases} m_1(\ddot{x}_1 + w) + c_1\dot{x}_1 - c_2(\dot{x}_2 - \dot{x}_1) + k_1x_1 - k_2(x_2 - x_1) = \\ = P_1(t) - u_1 + u_2 \\ \dots \\ m_i(\ddot{x}_i + w) + c_i(\dot{x}_i - \dot{x}_{i-1}) - c_{i+1}(\dot{x}_{i+1} - \dot{x}_i) + \\ + k_i(x_i - x_{i-1}) - k_{i+1}(x_{i+1} - x_i) = P_i(t) - u_j + u_{j+1} \\ \dots \\ m_n(\ddot{x}_n + w) + c_n(\dot{x}_n - \dot{x}_{n-1}) + k_n(x_n - x_{n-1}) = P_n(t) - u_r \end{cases} \qquad (2)$$

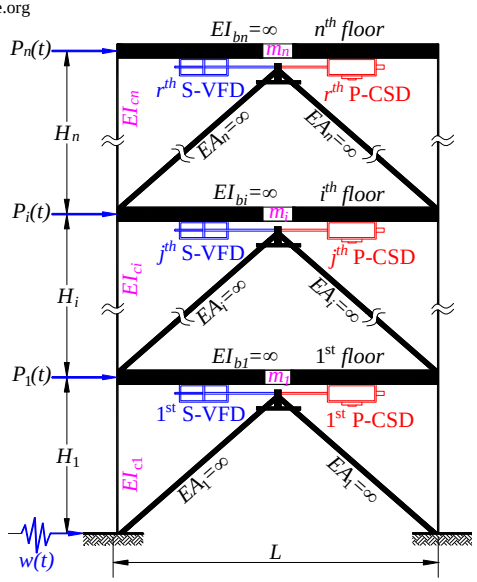

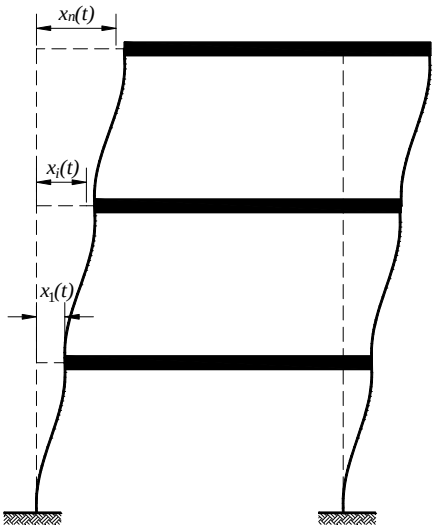

Fig 1: Multi-story shear frame equipped with P-VFDs and S-CSDs

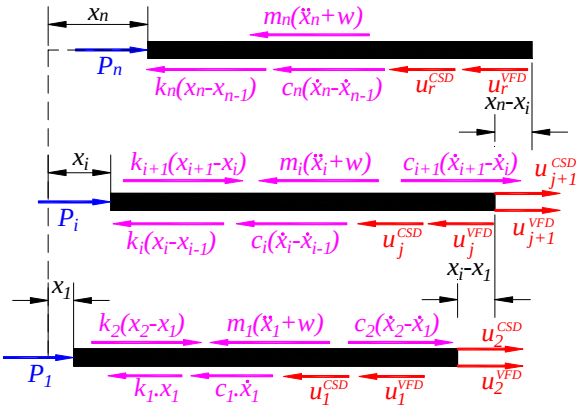

Fig 2: The free body diagram for structures with P-VFD and S-CSD

The lateral control force at the i^{th} floor u_j $(j=1,2,...,r)$ is the sum of P-VFD force $u_j^{\text{P-VFD}}$ and S-CSD $u_j^{\text{S-CSD}}$ force as

$$u_j = u_j^{\text{P-VFD}} + u_j^{\text{S-CSD}} \tag{3}$$

Passive viscous damper force $u_j^{\text{P-VFD}}$ generates at the i^{th} floor [3]

$$u_j^{\text{P-VFD}}(t) = C_i.\left|\dot{x}_i(t)-\dot{x}_{i-1}(t)\right|^{\alpha}.\text{sgn}\left[\dot{x}_i(t)-\dot{x}_{i-1}(t)\right] \tag{4}$$

where C_i is the viscous fluid damper coefficient; $\dot{x}_i(t)$ is the velocity at the i^{th} floor; α is a predetermined exponent. Usually for seismic application, $\alpha \square 1$, producing linear response.
The variable force developed by S-CSD at the i^{th} floor is given by [4]:

$$\begin{aligned} u_j^{\text{S-CSD}}(t) &= C_M\left[x_i(t)-x_{i-1}(t)+x_i^{ctr}(t)\right]+ \\ &+n_C C_C\left\{x_0-\left[x_i(t)-x_{i-1}(t)\right]\right\}\times \\ &\times\left\{\sqrt{\frac{\frac{a^2}{4}+x_0^2}{\frac{a^2}{4}+\left\{x_0-\left[x_i(t)-x_{i-1}(t)\right]\right\}^2}}-1\right\} \end{aligned} \tag{5}$$

where C_M and C_C are the stiffness coefficients of the main spring and the corrector, respectively; n_C is the number of stiffness correctors; $x_i(t)$ is the displacement; $x_i^{ctr}(t)$ is the displacement of the activating bar; x_0 is the horizontal projection of the corrector in the unloaded state; a is the diameter of the internal cylinder at the i^{th} floors.
On the ground of the characteristic of S-CSD, the displacement of the main spring is on elastic domain, hence, $x_i^{ctr}(t)$ must satisfy

$$x_{\text{limit}}^{c} \le x_i[k]-x_{i-1}[k]+x_i^{ctr}(t) \le x_{\text{limit}}^{t} \tag{6}$$

where $x_{\text{limit},c}$ and $x_{\text{limit},t}$ are the compression and tension linearly elastic limit of S-CSDs, respectively; $C_M, C_C, x_{\text{limit},c}$ and $x_{\text{limit},t}$ are taken as [5].
Conditions to generate semi-active control forces in S-CSD are

$$x_{\max}^{\text{top story}} \ge \frac{\sum_{\text{story}} H_i}{500} \tag{7}$$

Equation (2) can be written compactly as:

$$\mathbf{M}.\ddot{\mathbf{x}}+\mathbf{C}.\dot{\mathbf{x}}+\mathbf{K}.\mathbf{x}=\mathbf{F_d}.\mathbf{u}-\mathbf{M}.\mathbf{r}.w \tag{8}$$

where $\mathbf{M}=\begin{bmatrix} m_1 & 0 & 0 \\ \vdots & m_i & \vdots \\ sym & & m_n \end{bmatrix}\left(\mathbf{M}\in\square^{n\times n}\right)$;

$\mathbf{C}=\begin{bmatrix} c_1+c_2 & -c_2 & 0 & 0 & 0 \\ \cdots & & & & \\ 0 & -c_i & c_i+c_{i+1} & -c_{i+1} & 0 \\ \cdots & & & & \\ sym & & & -c_n & c_n \end{bmatrix}\left(\mathbf{C}\in\square^{n\times n}\right)$;

$\mathbf{K}=\begin{bmatrix} k_1+k_2 & -k_2 & & & \\ \cdots & & & & \\ & -k_i & k_i+k_{i+1} & -k_{i+1} & \\ \cdots & & & & \\ sym & & & -k_n & k_n \end{bmatrix}\left(\mathbf{K}\in\square^{n\times n}\right)$;

$\mathbf{r}=\begin{Bmatrix} 1 \\ \vdots \\ 1 \\ \vdots \\ 1 \end{Bmatrix}\left(\mathbf{r}\in\square^{n\times 1}\right)$; $\mathbf{x}=\begin{Bmatrix} x_1 \\ \vdots \\ x_i \\ \vdots \\ x_n \end{Bmatrix}\left(\mathbf{x}\in\square^{n\times 1}\right)$; $\dot{\mathbf{x}}=\frac{d}{dt}\mathbf{x}$;

$\ddot{\mathbf{x}}=\frac{d^2}{dt^2}\mathbf{x}$; $\mathbf{F_d}$ is a matrix indicating the position of r dampers P-VFD and r dampers S-CSD $\left(\mathbf{F_d}\in\square^{n\times r}\right)$ and $\mathbf{u}(t)=\left\{P_1(t)-u_1+u_2,...,P_i(t)-u_j+u_{j+1},...,P_n(t)-u_r\right\}^T$ presents the vector of the forces provided by the (VFD+CSD) and the lateral forces.

The notations $\in\square^{n\times r}$ indicate the dimension of a real-numbered matrix with n rows and r columns. Equation (8) is the equation of motion governing the displacement $x_i(t)$ of the idealized structure, assumed to be linearly elastic, subjected to an external dynamic force $P_i(t)$, and controlled by P-VFDs and S-CSDs.

2.2 Feature of Structures with P-VFD and S-CSD

With the structural system subjected to a seismic force as shown in Fig 1, the equation of motion of the system may be rewritten in a state space equation

$$\dot{\mathbf{z}}(t)=\mathbf{A}.\mathbf{z}(t)+\mathbf{B}.\mathbf{u}(t)+\mathbf{E}.w(t) \tag{9}$$

where the vector $\mathbf{z}(t)=\begin{Bmatrix}\mathbf{x}(t)\\ \dot{\mathbf{x}}(t)\end{Bmatrix}\left(\mathbf{z}(t)\in\square^{2n\times 1}\right)$ represents the state of the structure which contains the relative-to-ground velocities $\dot{\mathbf{x}}(t)$ and displacements $\mathbf{x}(t)$ of the structure; $\dot{\mathbf{z}}(t)=\frac{d}{dt}\mathbf{z}(t)$; $\mathbf{A}=\left[\begin{array}{c|c} \mathbf{0}_{n\times n} & \mathbf{I}_{n\times n} \\ \hline -\mathbf{M}^{-1}.\mathbf{K} & -\mathbf{M}^{-1}.\mathbf{C} \end{array}\right]$ $\left(\mathbf{A}\in\square^{2n\times 2n}\right)$ denotes the system matrix composed of the structural mass, damping and stiffness matrices;

$\mathbf{B} = \begin{bmatrix} \mathbf{0}_{n\times r} \\ \hline \mathbf{M}^{-1}.\mathbf{F}_{\mathbf{d}} \end{bmatrix} \left(\mathbf{B} \in \mathbb{R}^{2n\times r}\right)$ is the distribution matrix of the control forces; $\mathbf{E} = \begin{bmatrix} \mathbf{0}_{n\times 1} \\ \hline -r \end{bmatrix} \left(\mathbf{E} \in \mathbb{R}^{2n\times 1}\right)$ is the earthquake excitation.

The closed-loop feedback control is used in this paper; thus the active force matrix can be expressed as:

$$\hat{\mathbf{u}}(t) = -\mathbf{F}.\mathbf{z}(t) \qquad (10)$$

in which $\mathbf{F} \in \mathbb{R}^{r\times 2n}$ is matrix of feedback gain; $\hat{\mathbf{u}}(t) \in \mathbb{R}^{r\times 1}$

2.3 Determining the Active Feedback Gain [8]

2.3.1 Riccati Optimal Active Control Algorithm (ROAC)

In the Riccati Optimal Active Control algorithm, control force **u**(*t*) may be determined by minimizing a standard quadratic index, *J*, given by:

$$J = \frac{1}{2}\int_{t_0}^{t_f} \left[\mathbf{z}(t)^T\, \mathbf{Q}\, \mathbf{z}(t) + \hat{\mathbf{u}}(t)^T\, \mathbf{R}\, \hat{\mathbf{u}}(t)\right] dt \qquad (11)$$

where **Q** is a positive semi-definite symmetrical matrix $\left(\mathbf{Q} \in \mathbb{R}^{2n\times 2n}\right)$; **R** is an positive-definite symmetrical matrix so that all control forces are effective, $\left(\mathbf{R} \in \mathbb{R}^{r\times r}\right)$; performance index, *J*, represents a weighted balance between structural response and control energy. According to mechanic meaning, *J* is the energy the structure consume during the earthquake period. The Riccati equation:

$$\mathbf{PA} + \mathbf{A}^T\mathbf{P} - \mathbf{PBR}^{-1}\mathbf{B}^T\mathbf{P} + \mathbf{Q} = 0 \qquad (12)$$

Riccati matrix $\mathbf{P} \in \mathbb{R}^{2n\times 2n}$ in this equation is constant and can be solved by numerical methods. Then, the active control force matrix expressed by Equation (10) becomes:

$$\hat{\mathbf{u}}(t) = -\mathbf{R}^{-1}\mathbf{B}^T\mathbf{P}\, \mathbf{z}(t) = -\mathbf{F}\, \mathbf{z}(t) \qquad (13)$$

in which $\mathbf{F} \in \mathbb{R}^{r\times 2n}$ and $\mathbf{F} = \mathbf{R}^{-1}\mathbf{B}^T\mathbf{P}$ (14)

2.3.2 Pole Placement Algorithm

F is determined from solving the following equation

$$\left|s\mathbf{I} - \mathbf{A} + \mathbf{BF}\right| = (s - s_1)(s - s_2)...(s - s_n) \qquad (15)$$

where $s_i\ (i = 1, 2, \ldots, n)$ is chosen to be eigenvalues of matrix **A**; **F** is chosen so that $|\mathbf{A} - \mathbf{BF}|$ having its eigenvalues will be s_i

2.3.3 Instantaneous Control with Displacement and Velocity Feedback (ICDVF)

The feedback gain is given in a concise matrix form as follows:

$$\mathbf{F} = \mathbf{B}_2^{-1}\left[\mathbf{\Phi}_{2\mathbf{c}}.\mathrm{diag}\left(\lambda_i\right)_{\mathbf{c}} - \mathbf{A}_2.\mathbf{\Phi}_{\mathbf{c}}\right].\left(\mathbf{C}.\mathbf{\Phi}_{\mathbf{c}}\right)^{-1} \qquad (16)$$

Note that the dimension of **F** is $(r \times q)$, provided that *r* and *q* are the total numbers of control devices and measurement sensors used for control.

Where the diagonal matrix $diag\left(\lambda_i\right)_c \in \mathbb{R}^{q\times q}$ and the rectangular matrix $\Phi_{\mathbf{c}} \in \mathbb{R}^{2n\times q}$ contain the target eigenvalues and eigenvectors, respectively.

The matrices $\mathbf{A}_2 \in \mathbb{R}^{r\times 2n}$, $\mathbf{B}_2 \in \mathbb{R}^{r\times r}$ and $\mathbf{\Phi}_{2\mathbf{c}} \in \mathbb{R}^{r\times q}$ are the lower portions of the matrices **A, B** and $\mathbf{\Phi}_{\mathbf{c}}$; $\mathbf{C} \in \mathbb{R}^{q\times 2n}$ denotes the sensor placement matrix. Each set of target modal values are then converted into one pair of the conjugated target eigenvalues by the following equations:

$$\lambda_{\substack{2i-1 \\ 2i}}^{(c)} = -\zeta_i.\omega_i \pm j.\omega_i\sqrt{1-\zeta_i^2} \qquad (17)$$

2.3.4 Instantaneous Optimal Active Closed-Loop Control Algorithm (IOAC)

In the IOAC algorithm, optimal control force matrix $\mathbf{u}(t)$ is determined by minimizing an instantaneous time-dependent performance index $J_P(t)$ rather than ROAC integral performance index *J*:

$$J_P(t) = \mathbf{z}(t)^T\, \mathbf{Q}\, \mathbf{z}(t) + \hat{\mathbf{u}}(t)^T\, \mathbf{R}\, \hat{\mathbf{u}}(t) \qquad (18)$$

The optimal control force $\hat{\mathbf{u}}(t)$ depends on the time interval Δt, $t_0 \le t \le t_f$ and is given by:

$$\hat{\mathbf{u}}(t) = -\left(\frac{\Delta t}{2}\right)\mathbf{R}^{-1}\mathbf{B}^T\mathbf{Q}\, \mathbf{z}(t) = -\mathbf{F}.\mathbf{z}(t) \qquad (19)$$

with $\mathbf{F} = \left(\frac{\Delta t}{2}\right)\mathbf{R}^{-1}\mathbf{B}^T\mathbf{Q}$ (20)

2.4 A Numerical Time-Stepping Method for Solving the State Space Motion

In solving the state space motion (9), a numerical method ZOH (Zero Order Hold) is used to find the dynamic analysis because earthquake excitation varies arbitrarily with time. The applied force, control force, and ground acceleration are given by a set of discrete values and assumed to be constant within any time interval, the solution of Equation (9) is written in an incremental form [8]:

$$\mathbf{z}[k+1] = \mathbf{A}_{\mathbf{d}}.\mathbf{z}[k] + \mathbf{B}_{\mathbf{d}}.\mathbf{u}[k] + \mathbf{E}_{\mathbf{d}}.\mathbf{w}[k] \qquad (21)$$

with $\begin{cases} \mathbf{A_d} = e^{\mathbf{A}.\Delta t} \\ \mathbf{B_d} = \mathbf{A}^{-1}(e^{\mathbf{A}.\Delta t} - \mathbf{I})\mathbf{B} \\ \mathbf{E_d} = \mathbf{A}^{-1}(e^{\mathbf{A}.\Delta t} - \mathbf{I})\mathbf{E} \end{cases}$

Equation (21) states that the structural response of the next time step $\mathbf{z}[k+1]$ can be evaluated based on the current time step information of $z[k], u[k]$ and $w[k]$.

The active control force $\hat{\mathbf{u}}(\mathbf{t})$ can be obtained from one of the four algorithms and then P-VFD and S-CSD forces are taken as this active control force. Fig 3 and

Fig 4 depicts the block diagram of the system controlled by P-VFDs and S-CSDs.

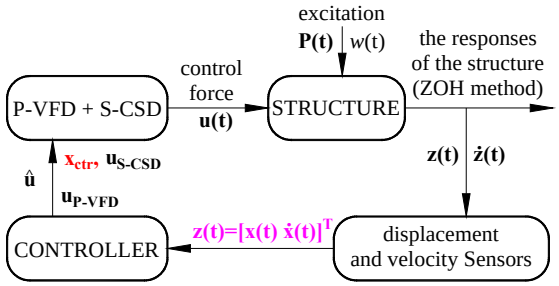

Fig 3: Hybrid controlled structural system with (VFD+CSD)

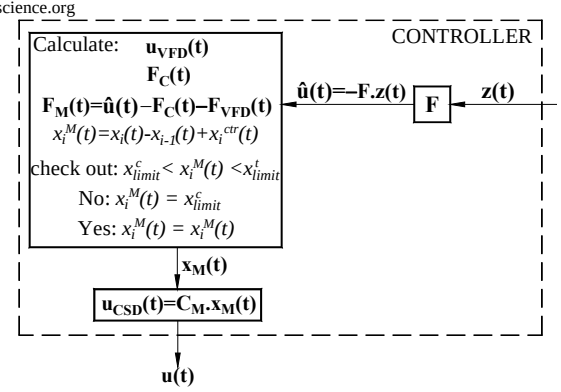

Fig 4: Controller block

3. NUMERICAL EXAMPLE

The three-, nine-, and twenty-story structures used for this benchmark study were designed for the SAC Phase II Steel Project [9]. Although not actually constructed, these structures meet seismic code and represent typical low-, medium-, and high-rise buildings designed for the Los Angeles, California region. These buildings were chosen because they also serve as benchmark structures for the SAC studies and will provide a wider basis for the comparison of results. The specifications for each of these buildings are discussed in the following paragraphs.

The seismic mass at the i^{th} floor of systems: $m_1 = m_2 = 957\times10^3\,(kg); m_3 = 1040\times10^3\,(kg)$

The determination of stiffness of three-story benchmark buildings are taken as the following table [6]:

Table I: The stiffness properties of three-story benchmark building

Columns ID	Stiffness Properties				
	Section Name	I_c (cm^4)	H (cm)	E $\left(kN/cm^2\right)$	$\frac{12.EI_c}{H^3}$ $\left(kN/cm\right)$
(1),(4)	W14×257	141,519	396	2×10^4	547
(2),(3)	W14×311	180,228	396		697
(5)	W14×68	30,094	396		116

Then,

$k_1 = k_2 = k_3 = 547\times2 + 697\times2 + 116 = 2603\left(\frac{kN}{cm}\right)$. The mass and stiffness matrices are shown as

$$\mathbf{M} = \begin{bmatrix} 957 & & \\ & 957 & \\ & & 1040 \end{bmatrix} \times 10^3\,(kg);$$

$$\mathbf{K} = \begin{bmatrix} 2 & -1 & 0 \\ -1 & 2 & -1 \\ 0 & -1 & 1 \end{bmatrix} 2603\times10^5 \left(\frac{N}{m}\right)$$

The natural frequencies of the structure are:

$\omega_1 = 7.17\left(rad/s\right)$; $\omega_2 = 20.27\left(rad/s\right)$; $\omega_3 = 29.59\left(rad/s\right)$ or

$T_1 = 0.876(s)$; $T_2 = 0.310(s)$; $T_3 = 0.212(s)$

The damping ratios of the bare steel frame for the first and second modes are $\zeta_1 = \zeta_2 = 5\%$. Derived from Rayleigh procedures [6], damping matrix is

$$\mathbf{C} = \begin{bmatrix} 24.04 & -9.48 & 0 \\ -9.48 & 24.04 & -9.48 \\ 0 & -9.48 & 14.99 \end{bmatrix} \times 10^5 \left(\frac{N.s}{m} \right)$$

Similarly, the dynamic properties of the nine- and twenty-story benchmark buildings are given by the following tables

Table II: The dynamics properties of the nine-story building

i^{th} Floor	1st	2nd	3rd	4th	
$m_i \left(\times 10^3 kg\right)$	1010	989	989	989	
	5th	6th	7th	8th	9th
	989	989	989	989	1070
i^{th} Floor	1st	2nd	3rd	4th	
$k_i \left(\times 10^3 kN/cm\right)$	10,260	23,942	23,942	18,115	
	5th	6th	7th	8th	9th
	18,115	12,787	12,787	11,322	11,322

Table III: The dynamics properties of the twenty-story building

i^{th} Floor	1st	2nd – 4th	5th – 10th	11th – 13th
$m_i \left(\times 10^3 kg\right)$	2,815	2,760	2,760	2,760
	14th – 16th	17th – 18th	19th	20th
	2,760	2,760	2,760	2,920
i^{th} Floor	1st	2nd – 4th	5th – 10th	11th – 13th
$k_i \left(\times 10^3 kN/cm\right)$	14,871	39,625	25,472	20,848
	14th – 16th	17th – 18th	19th	20th
	13,384	11,784	7,892	7,892

The control parameters of P-VFDs and S-CSDs for three typical buildings are referred to data of manufactures [3] and in an effort to compare results. Thus, P-VFDs' coefficient is $C_i^{VFD} = 10^6 \left(Ns/m \right)$ [3] and the stiffness of S-CSDs' main spring at the i^{th} floor with its code 4052 is $C_i^M = 4662 \times 10^3 \left(N/m \right)$ and $x_{\text{limit}} = \pm 0.0035m$ [4].

The vital dynamic responses of structure which needs to be evaluated are roof displacement, shear force at the first floor, and the top floor's acceleration.

3.1 Response of the Three-Story Building Subjected to ElCentro Earthquake

The first benchmark structure representing low buildings is analyzed. This structure is equipped with one P-VFD and one S-CSD at each floor and subjected to ElCentro earthquake excitation.

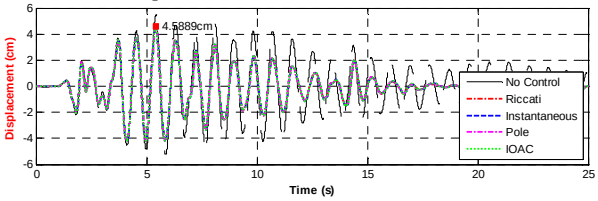

Fig 5: Roof displacement response of the structure of four algorithms

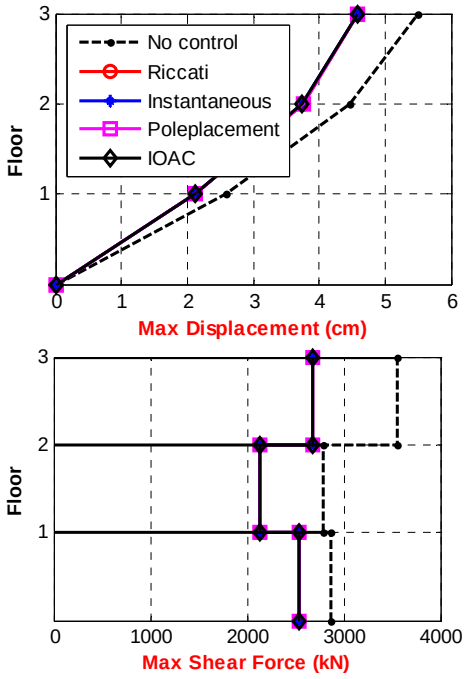

Fig 6: Maximum displacement and shear force responses of the structure with four algorithms (Riccati, Instantaneous, Pole placement and IOAC)

Table IV: The dynamics properties of the twenty-story benchmark building with Riccati algorithms

Cases	$C_i^{VFD}\left(\frac{N.s}{m}\right)$, $C_i^M\left(\frac{N}{m}\right)$	$x_3^{\max}$ (cm) (Reduction %)	$SF_1^{\max}$ $\left(\times 10^3 kN\right)$ (Reduction %)	$\frac{a_3^{\max}}{g}$ (Reduction %)
	No control	5.5019 (0%)	2.8645 (0%)	0.5128 (0%)
(1)	1×10^6, 4662×10^3	4.5889 (17%)	2.5397 (11%)	0.5170 (-1%)
(2)	2×10^6, 4662×10^3	4.0314 (27%)	2.3045 (20%)	0.5164 (-1%)

(3)	3×10^6, 4662×10^3	3.8138 (31%)	2.0908 (27%)	0.5134 (0%)
(4)	4×10^6, 4662×10^3	3.6422 (34%)	1.9015 (34%)	0.5089 (1%)
(1)	10^6, $4662\times10^3\times1$	4.5889 (17%)	2.5397 (11%)	0. 5170 (-1%)
(5)	10^6, $4662\times10^3\times2$	4.3179 (22%)	2.5297 (12%)	0.5181 (-1%)
(6)	10^6, $4662\times10^3\times3$	4.0404 (27%)	2.5202 (12%)	0.5192 (-1%)
(7)	10^6, $4662\times10^3\times4$	3.8428 (30%)	2.5135 (12%)	0.5199 (-1%)

Fig 5 and Fig 6 shows that the four active control algorithms used to control the S-CSDs of the structure produce the same response reduction. The lines representing the four algorithms are almost coincided in these figures. Moreover, speaking of energy loss, the area of the P-Table IV and Fig 7). Among these cases, the response reduction of the structure may be improved by using more P-VFDs or by attaching S-CSDs with higher capacity.

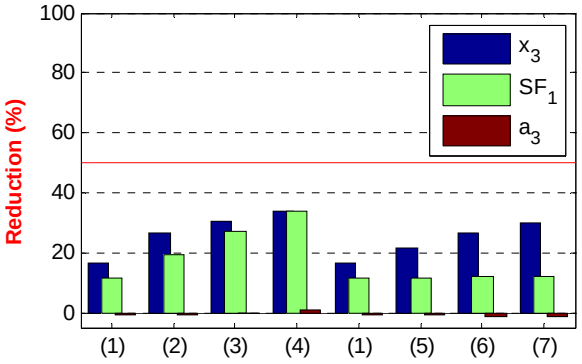

Fig 7: The response reduction of the structure with changing C_i^{VFD} and C_i^M

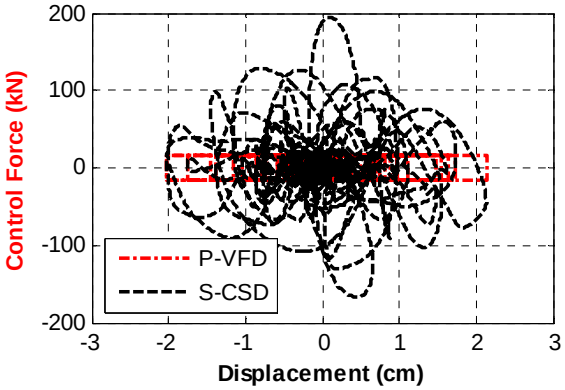

Fig 8: Force-deformation hysteresis loop of (1) for the 1st floor

VFD's hysteresis loop is bigger than that of the S-CSD's one (Fig 8), therefore, energy dissipated by the P-VFD is more than that by the S-CSD (Fig 9). Besides, the response reductions of the structure with the hybrid control are negligible (

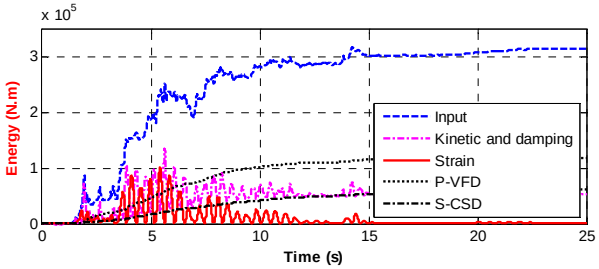

Fig 9: The energy of the three-story building

3.2 Response of the Nine-Story Building Subjected to Kobe Earthquake

The next structure, the nine-story building, representing typical medium buildings is mentioned in this subsection. This structure is equipped with one P-VFD and five S-CSDs at each floor and subjected to Kobe earthquake excitation. The dynamic response of the structure is shown

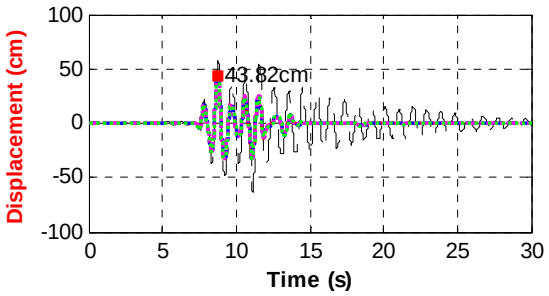

Fig 10: The roof displacement response

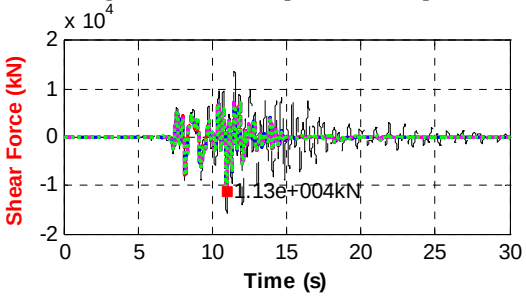

Fig 11: The roof shear force response

First of all, all four algorithms give the same response. Additionally, the maximum response reduction in the cases (A), (B) and (C) is still low – approximately 40% (

Fig 13, Fig 14, and Fig 15), but the average response reduction is reasonable – more 60%. The good average response reduction makes the vibration of system decay after several periods (

Fig 10). Furthermore, the combination of the P-VFD and the S-CSD for hybrid control gives the best reduction. This combination not only improves the seismic damping capacity but also is an optimal choice to reach the cost-effective target.

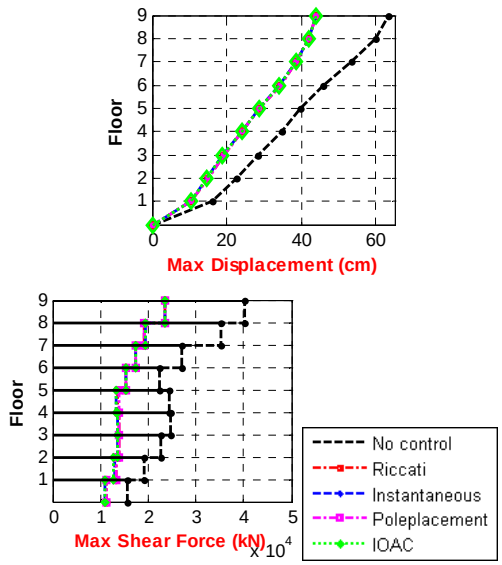

Fig 12: The maximum displacement and shear force responses with the four algorithms

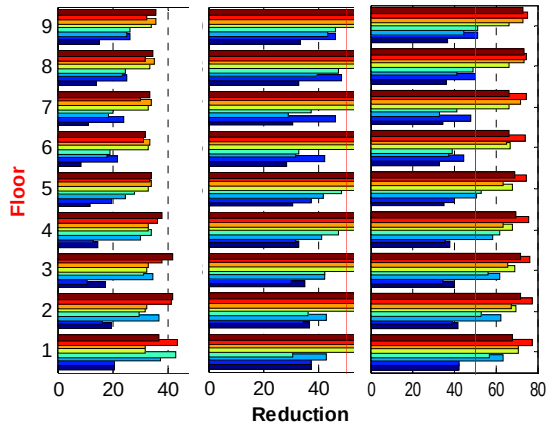

Fig 13: Only using 6 P-VFDs at each floor - case (A)

Fig 14: Only using 6 S-CSDs at each floor - case (B)

Fig 15: Combination of the P-VFD and the S-CSD - case (C)

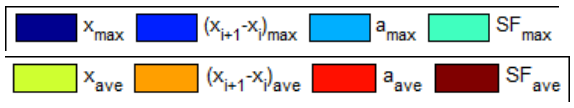

3.3 Response of the Twenty-Story Building Subjected to Kobe earthquake

The last structure, the twenty-story buildings, representing high-rise buildings is analyzed in the last subsection. This structure is installed with six P-VFDs and six S-CSDs at each floor and subjected to Kobe earthquake excitation.

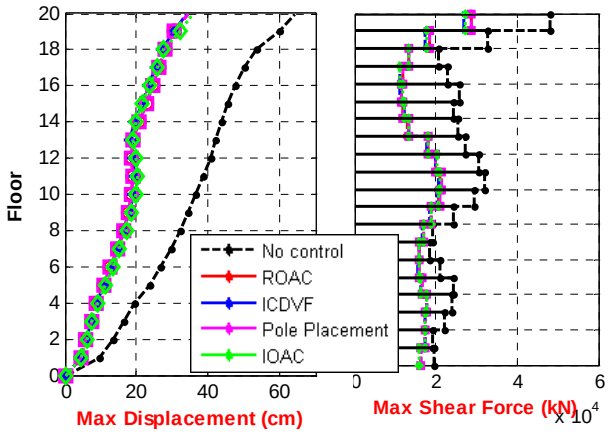

Fig 16: The max displacement and shear force responses of the structure

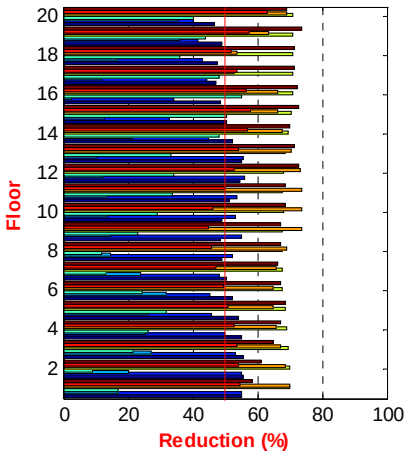

Fig 17: The response reduction of the structure

Fig 16 shows the peak value of displacement and shear force responses. The figure indicates the same response of four active control algorithms. There is not much difference of responses between the algorithms. In addition, the response reduction (Figure 17) of the high-rise building subjected to high peak ground acceleration Kobe earthquake is quite reasonable. The average reduction reaches approximately 70 percent.

In an attempt to investigate the effectiveness of response reductions of the structure, simulations were carried out on two solutions: (D) using the combination of P-VFDs and S-CSDs; traditional solution (E); and an increase in the column's stiffness to eight times to

achieve the desired response. The column's stiffness of system is calculated by (1).

Table 5: Column section property type of each solution, wide flange section

i^{th} *floor*	Solution (D)			
	property type	$I_{c,i}\left(cm^4\right)$	Section $A\ (cm^2)$	$k_i\left(\times 10^4 \frac{kN}{cm}\right)$
1	W24x335	495315	634.8	1.487
2	W24x335	495315	634.8	3.962
3	W24x335	495315	634.8	3.962
4	W24x335	495315	634.8	3.962
5	W24x229	318417	433.5	2.547
6	W24x229	318417	433.5	2.547
7	W24x229	318417	433.5	2.547
8	W24x229	318417	433.5	2.547
9	W24x229	318417	433.5	2.547
10	W24x229	318417	433.5	2.547
11	W24x192	260560	363.2	2.085
12	W24x192	260560	363.2	2.085
13	W24x192	260560	363.2	2.085
14	W24x131	167325	248.4	1.338
15	W24x131	167325	248.4	1.338
16	W24x131	167325	248.4	1.338
17	W24x117	147345	221.9	1.178
18	W24x117	147345	221.9	1.178
19	W24x84	98646	159.4	0.789
20	W24x84	98646	159.4	0.789
		TOTAL	**7,737.6**	

i^{th} *floor*	Solution (E)			
	property type	$I_{c,i}\left(cm^4\right)$	Section $A\ (cm^2)$	$k_i\left(\times 10^4 \frac{kN}{cm}\right)$
1	2xW36x848	4,070,743	2,451.6	12.222
2	2xW36x848	4,070,743	2,451.6	32.566
3	2xW36x848	4,070,743	2,451.6	32.566
4	2xW36x848	4,070,743	2,451.6	32.566
5	2xW30x526	2,439,116	1,987.0	19.513
6	2xW30x526	2,439,116	1,987.0	19.513
7	2xW30x526	2,439,116	1,987.0	19.513
8	2xW30x526	2,439,116	1,987.0	19.513
9	2xW30x526	2,439,116	1,987.0	19.513
10	2xW30x526	2,439,116	1,987.0	19.513
11	2xW27x539	2,122,780	2,038.8	16.982
12	2xW27x539	2,122,780	2,038.8	16.982
13	2xW27x539	2,122,780	2,038.8	16.982
14	2xW24x450	1,423,512	1,703.2	11.388
15	2xW24x450	1,423,512	1,703.2	11.388
16	2xW24x450	1,423,512	1,703.2	11.388
17	2xW24x408	1,257,018	1,535.4	10.056
18	2xW24x408	1,257,018	1,535.4	10.056
19	2xW24x279	799,164	1,058.0	6.393
20	2xW24x279	799,164	1,058.0	6.393
			38,141.2	

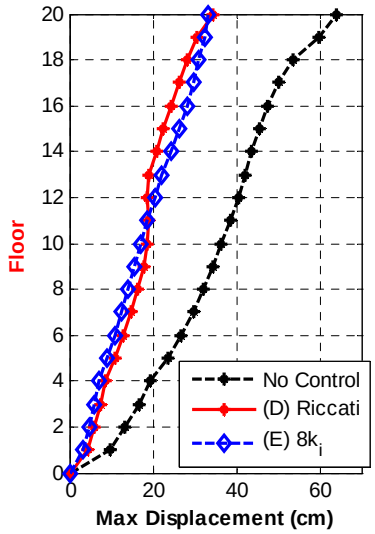

Fig 18: The peak displacement response

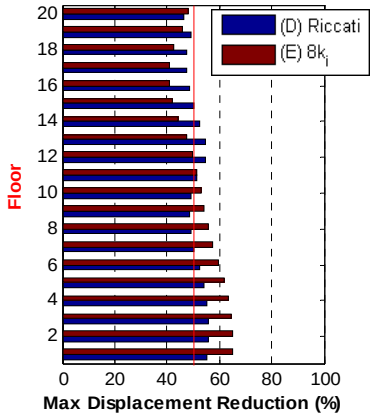

Fig 19: The peak displacement reduction

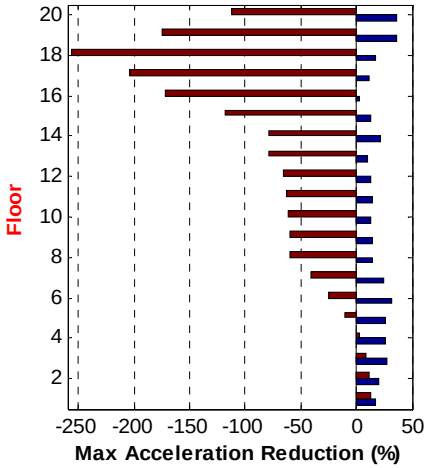

Fig 20: The peak acceleration reduction

As the column's stiffness of structure increases eight times, the displacement is also enhanced, corresponding to the column's stiffness (

Fig 18 and

Fig 19). Also, the acceleration response reduction is negative (

Fig 20); the increase in the columns stiffness causes higher acceleration to the system because the structure is now stiffer. Moreover, the max shear force response of solution (D) and (E) look nearly the same, but in order to get that reduction, the column's stiffness of the structure in solution (E) must be increased by eight times. It means the steel material used for this building upgrades, up to $\frac{38{,}141.2}{7{,}737.6} = 4.93$ times, i.e. the costs were cut by 79.7 percent.

4. CONCLUSION

Used to control S-CSDs, the four active algorithms give the same efficiency in reducing responses including displacement, acceleration, and shear forces. When the structures, benchmark buildings, are subject to weak earthquake excitation and equipped with P-VFDs and S-CSDs, the dissipation of energy is principally the task of P-VFDs. With S-CSDs joining with P-VFDs , the response reduction significantly increases efficiency. Furthermore, this paper introduces another option for structural control, the hybrid control. To avoid costly consumption during operating and maintaining systems as well as to have the desired effect, the use of P-VFDs and S-CSDs at the same time is an optimal choice. Last but not least, using P-VFDs and S-CSDs for high-rise buildings is sound for Vietnam condition.

REFERENCES

[1] Chu Quoc Thang, Pham Nhan Hoa, and Dang Duy Khanh – Passive control of structures with controlled stiffness devices and viscous fluid dampers combined – The 10th National Mechanics Solid Conference, pp. 698-704, Thai Nguyen, Viet Nam, December 2010

[2] T.T. Soong and B.F. Spencer – Supplemental energy dissipation: state-of-the-art and state-of-the practice – Engineering Structures 24, 243–259, 2002

[3] Robert J. MCNAMARA and Douglas P. Taylor – Fluid viscous dampers for high-rise buildings – The structural design of tall and special buildings – 12, 145–154, 2003

[4] Y. Ribakov – Semi-Active predictive control of nonlinear structures with controlled stiffness devices and friction dampers – Structural design Tall Special Buildings 13, pp. 165-178, 2004

[5] Website: http://www.globalspec.com/

[6] Anil K.Chopra – Dynamics of Structures, 2nd editor – Prentice Hall Press – 2001

[7] Lyan-Ywan Lu – Predictive control of seismic structures with semi-active friction dampers – Earthquake Engineering Structures – Dynamics. 2004; 33:647–668

[8] Meirovitch. L – Dynamics and Control of Structures – John Wiley & Sons, New York, 1990.

[9] Y.Ohtori, R. E. Christenson, B. F. Spencer – Benchmark Control Problems for Seismically Excited Nonlinear Buildings – Journal Of Engineering Mechanics © ASCE / April 2004.

AUTHOR PROFILES

Angeli Doliente Cabaltica received her Master degree in Environmental Sanitation from Gent, Belgium in 2007 and in Water Resources Engineering and Management from Stuttgart, Germany in 2011. Currently, she is a lecturer at the International University – Vietnam National University, Vietnam.

Pham Nhan Hoa received the master degree in civil engineering from Liege, Belgium in 2006. Currently, he is a lecturer at the International University – Vietnam National University, Vietnam.

Chu Quoc Thang received the PhD degree in structural engineering from TTI, Hungary in 1987. Currently, he is an Associate Professor at the International University – Vietnam National University, Vietnam.